Axisymmetric instabilities between coaxial rotating disks

By JEAN PÉCHEUX and E. FOUCAULT

Laboratoire d'Etudes Aérodynamiques (UMR CNRS 6609), Université de Poitiers,
Boulevard Marie et Pierre Curie, Téléport 2, BP 30179,
86962 Futuroscope Chasseneuil Cedex, France

This paper concerns the stability of the von Kármán swirling flow between coaxial disks. A linear stability analysis shows that for moderate Reynolds numbers ($Re \leqslant 50$) and for any rotation ratio $s \in [-1, 1[$ there is a radial location r_{pc} from which the self-similar von Kármán solutions become unstable to axisymmetric disturbances. When the disks are moderately counter-rotating ($s \in [-0.56, 0[$), two different disturbances (types I and II) appear at the same critical radius. A spatio-temporal analysis shows that, at a very short distance from this critical radius, the first disturbance (type I) becomes absolutely unstable whereas the second (type II) remains convectively unstable. Outside this range of aspect ratios, all the disturbances examined are found to be absolutely unstable. The flow between two coaxial rotating disks enclosed in a stationary sidewall is then numerically investigated. For sufficently large aspect ratios, the cavity flow is found to be globally unstable for axisymmetric disturbances similar to that calculated with the self-similar solutions. The flow in cavities with aspect ratios smaller than $R \approx 10.3$ (and $Re \leqslant 50$) is not destabilized by these axisymmetric disturbances. An experimental investigation conducted for a cavity with aspect ratio $R = 15$ confirms the numerical results. Axisymmetric disturbances similar to those calculated for the same cavity are detected and three-dimensional modes can also be observed near the sidewall.

1. Introduction

It is unnecessary to point out the importance of the flows in rotating cavities because of the many industrial configurations in which they are encountered (e.g. turbo-machinery) and their fundamental interest (e.g. models for three-dimensional flows). Flows between rotating disks can be represented by self-similar functions (in the case of infinite disks) which are exact solutions to the complete Navier–Stokes equations for steady laminar flow (von Kármán 1921). These self-similar solutions have been calculated for many configurations between two coaxial infinite disks: one stationary and one rotating disk, and two co- or counter-rotating disks. Self-similar solutions can also be used to analyse the structures of the boundary layers near the disks (Bödewadt 1940; Batchelor 1951; Stewartson 1953) which constitute a good model for the study of swept-wing boundary layers. In these high-Reynolds-number cases, many authors have shown the existence of multiple solutions (e.g. Mellor, Chapple & Stokes 1968; Nguyen, Ribault & Florent 1975; Holodniok, Kubicek & Hlavacek 1977, 1981) and the question of their existence (independently of their stability) arose naturally for the flows between rotating disks in cavities.

Following Gregory, Stuart & Walker (1955), many authors have studied the stability of the flow in the vicinity of an infinite rotating disk. It has been shown that the first instability, of inflectional type, appears in the shape of quasi-stationary spirals in the frame of the disk. Other works have confirmed and clarified the nature of this instability in the case of two rotating disks (e.g. Faller & Kaylor 1966; Szeri *et al.* 1983*a, b*). A review of numerous studies up to the 1980s devoted to boundary layers of the rotating disks can be found in Reed & Saric (1989) or Owen & Rogers (1989). Moreover Szeto (1978) described the many existing solutions as a function of the Reynolds number and the rotation ratio *s* for two disks of infinite extent. In order to do this, linear stability analysis of the von Kármán self-similar solutions was performed with equally self-similar disturbances. He showed a stability diagram with the different solutions as a function of the Reynolds number $Re \leqslant 1000$ ($Re = \omega^* e^{*2}/\nu^*$ where ω^* is the tangential velocity of the upper disk, e^* the gap width between the two disks and ν^* the kinematic viscosity) and of the rotation ratio between the two disks ($|s| \leqslant 1$). For all values of the rotation ratio *s*, the von Kármán steady axisymmetric solution is found to be stable for $Re \leqslant 55$ towards self-similar disturbances. A linear stability analysis of the flow between a rotating and a stationary disk was conducted by San'kov & Smirnov (1992). Following the studies of Szeri *et al.* (1983*b*) and using the similarity solution as basic flow, they found several instabilities and that for low *Re* values the most dangerous disturbances are axisymmetric. They argued that there is always a critical $r_{pc} = r^*/e^*$ radius beyond which the flow becomes unstable and concluded that as *Re* tends towards zero, $r_{pc} \simeq 7820 Re^2$.

A very important theoretical study on the laminar–turbulent transition of the boundary layer of a rotating disk was conducted by Lingwood (1995). By applying the Briggs–Bers criterion (Briggs 1964; Bers 1975; Huerre & Monkewitz 1990) it is shown that above a local Reynolds number of $Re_p = 510$ (where $Re_p = r_p^* L^* \omega^*/\nu^*$ with $L^* = \sqrt{\nu^*/\omega^*}$ the boundary-layer thickness and r_p^* the local radius) an absolutely unstable disturbance appeared which caused the onset of transition to turbulence. This theoretical value of the transitional local Reynolds number is very close to the value generally observed in experiments, around 513. It is also shown that this absolute instability has an inertial origin and comes neither from the Coriolis effects nor from streamline curvature effects. These theoretical results were confirmed by the experimental study subsequently carried out by Lingwood (1996). The evolution of disturbances introduced locally into the boundary layer over a disk rotating in a still medium is examined. When an impulse at a radius lower than the value at which the laminar–turbulent transition is observed disturbs the boundary layer, a wave packet is convected outwards. Among the excited frequencies emerge two families predicted by linear-stability theory and convected at the same speed towards the periphery. However, the propagation velocity of the trailing edge of the wave packet decreases as the radius increases, until it reaches zero when a local Reynolds number of 510 is attained, thus defining the critical local radius where the flow becomes absolutely unstable. Lingwood then explains the transition to turbulence in the boundary layer of a rotating disk by an accumulation of energy at this critical radius from which the flow becomes absolutely unstable. A review of works devoted to rotating disks and their boundary layers can be found in Saric, Reed & White (2003).

Many other experimental studies have been devoted to the stability of the flows between coaxial disks. The destabilization of the basic flow between a stationary and a rotating disk enclosed by a stationary sidewall was particularly well studied by Gauthier, Gondret & Rabaud (1999); Schouveiler *et al.* (1999, 2001). The first instability observed appears as circular rolls, travelling towards the centre,

in the boundary layer of the stationary disk, when the Ekman and Bödewadt boundary layers are clearly separate. It appears for relatively high-Reynolds-number values, depending on the aspect ratio $R = R^*/e^*$ (where R^* is the radius of the disks); e.g. $Re \approx 75$ and $R = 20.9$ in Gauthier *et al.* (1999). It was shown that this primary supercritical bifurcation occurs for increasing Reynolds number values while preserving axisymmetry and it was suggested that this is due to the shear instability of the radial velocity profile. These studies were then extended to the flow between two co- or counter-rotating disks enclosed in a cavity (e.g. Iglesias & Humphrey 1998; Gauthier *et al.* 2002). Gauthier *et al.* (2002) present an experimental diagram of the various modes observed as a function of the relative rotation of each of the two disks for a high aspect ratio ($R = 20.9$). The cases of co-rotating and slightly counter-rotating disks behave as the rather similar and better known rotor–stator case (Gauthier *et al.* 1999; Serre, Crespo del Arco & Bontoux 2001), from the point of view of the basic flow on the one hand and the form of the first instability, which is always axisymmetric, on the other. The strongly counter-rotating case, however, is more complex and leads to structures of a new type, named *negative spirals*, which are described. For the exactly counter-rotating case, the first instability is observed even from $Re = 20$, i.e. well before the formation of the boundary layers near each of the two disks. It should be noted that only Gauthier *et al.* (2002) observe the destabilization of the basic flow by three-dimensional structures (but in the strongly counter-rotating case only) and also that their experimental device has a sidewall which moves with the higher disk and gives a particular basic flow.

At the same time, the stability of the flow in a cavity was studied numerically with axisymmetric codes. This assumption of axisymmetry is indeed justified by the experimental observations quoted previously which show that the basic flow is initially destabilized by circular waves (at least when the rotation ratio s is not too close to -1, if one takes into account the observations of Gauthier *et al.* 2002). In a certain number of studies, direct numerical simulation by means of spectral methods has been used (see Hill & Ball 1997; Cousin-Rittemard, Daube & Le Quéré 1998; 1999). The transitions are generally observed to occur by means of Hopf bifurcation. In the rotor–stator case ($s = 0$), Cousin-Rittemard *et al.* (1998) showed that in the boundary-layer regime, the basic flow lost stability via various scenarios depending on the curvature effects (the latter are governed by the inner to outer radii ratio $\delta = R_i/R$ with $\delta \to 1$ for a Cartesian cavity and $\delta = 0$ for disk systems including the rotation axis). These results were then confirmed by three-dimensional direct numerical simulations. Several types of instability were listed between a stationary and a rotating disk in a cylindrical cavity including the rotation axis ($\delta = 0$) and in an annular cavity radially confined by a shaft and a shroud ($\delta \neq 0$), in particular by Serre *et al.* (2001). For moderate aspect ratios, the influence of the curvature and confinement effects was evaluated by varying the geometric parameters δ and R. The basic flow is stationary and axisymmetric, of Batchelor type with a core of inviscid fluid in the centre of the cavity. The results confirm those already published, both experimental and numerical axisymmetric. The basic solution is found to be stable up to a critical Reynolds number Re_c such as $Re_c R^{1.8} = 10^4$. Beyond this, it is replaced by an unsteady solution with axisymmetric and/or three-dimensional structures, according to the value of the parameters. The numerical study of Nore *et al.* (2003) describes the first stages of the transition to turbulence in exactly counter-rotating cavities ($s = -1$) with a very small aspect ratio ($R = 0.5$). The computational code, also unsteady and three-dimensional, shows that the axisymmetric basic flow becomes unstable for notably high-Reynolds-number values ($Re/4 = 349$), under the

effect of a Kelvin–Helmholtz type mechanism. Then various structures of complex flows appear successively as *Re* is increased. Nore *et al.* (2004) extended this work to slightly larger aspect ratios, i.e. $R \in [0.5, 1.5]$. Again by means of a three-dimensional computational code, they find that for exactly counter-rotating disks ($s = -1$), the steady non-axisymmetric modes are the most unstable, but that the critical tangential wavenumber increases with the aspect ratio R. In an attempt to connect the unsteady three-dimensional solutions calculated with experimental observations (e.g. Gauthier *et al.* 2002; Schouveiler *et al.* 1999), they also examine the instability to axisymmetric disturbances, but find that for this range of aspect ratio their threshold is always higher than that of the non-axisymmetric modes, thus highlighting the importance of R for the selection of the most unstable modes. Moisy *et al.* (2004) studied both numerically and experimentally, an even broader range of aspect ratios: $R \in [2, 21]$. Their work was, however, limited to the boundary-layer type flow (i.e. with relatively high rotation rate) and, following Gauthier *et al.* (2002), they considered only configurations in which the sidewall rotates with the higher disk and thus the flow no longer closely resembles von Kármán swirling flows. They also found that instabilities are always of the Kelvin–Helmholtz type and that the curvature effects play only a minor part. Several instabilities of polygonal forms similar to those described by Lopez *et al.* (2002) and surrounded by a set of spiral arms, similar to those initially described by Gauthier *et al.* (2002), are calculated.

Instabilities in rotating flows can appear with several patterns according to the imposed conditions. In the particular case of rotating cavities, self-similar solutions may closely represent the flow when the aspect ratio R is high enough and when the edge effects are small enough. Then, instabilities in a cavity can be predicted well in the framework of linear stability theory. It is thus justified, as an initial stage, to examine the von Kármán swirling flow stability with respect to axisymmetric disturbances. It is necessary, however, to bear in mind that the flow can also be destabilized by three-dimensional disturbances, and this is undoubtedly the case when R is small, even if the boundary value of R remains to be determined.

This paper is devoted to the loss of stability of an incompressible viscous fluid flow between two parallel coaxial disks. In §2, it is shown that self-similar solutions become locally unstable for very moderate Reynolds-number values, long before the formation of the boundary layers. After a short introduction to the method used, the general characteristics of temporal and then spatio-temporal instability between co- and counter-rotating disks are presented. The study is limited to the first bifurcation of the solutions within the framework of axisymmetric disturbances and establishes a connection between the critical Reynolds number and the rotation rate $s \in [-1, 1[$. Then in §3, the characteristics of the solutions found to be unstable in the case of infinite disks are compared with the corresponding solutions (calculated by DNS) in a realistic interdisk cavity, i.e. between disks limited by a fixed sidewall. The particular case $R = 15$ and $s = -1$ is examined in more detail and the calculations compared with experimental results. Finally §4, reports the conclusions of this work.

2. Von Kármán flow between two rotating disks

The disks are modelled as two infinite planes with a gap width e^*, rotating around a common vertical axis z^* at a constant angular velocity $\omega^*(z^* = e^*)$ and $s\omega^*(z^* = 0)$ with $s \in [-1, 1[$, respectively. The origin of the cylindrical coordinates (r^*, θ, z^*) is located at the lower disk centre. The steady basic flow is given by von Kármán's exact

similarity solution to the Navier–Stokes equations. The approach used here is similar to that indicated by Lingwood (1995); the stability is examined locally by imposing infinitesimal disturbances at a distance r_p^* from the origin on the basic flow. Both basic flow and disturbances are assumed to be axisymmetric.

The length, velocity, time and pressure are non-dimensionalized by e^*, $e^*\omega^*$, $1/\omega^*$ and $\rho^* e^{*2}\omega^{*2}$, respectively. The equations governing the problem show three dimensionless parameters: $Re = \omega^* e^{*2}/\nu^*$, s and $r_p = r_p^*/e^*$. Near the loss of stability of the basic flow $(\bar{\boldsymbol{v}}, \bar{p})$, the instantaneous non-dimensional velocity and pressure are given by:

$$\boldsymbol{v}(t, r, z) = \bar{\boldsymbol{v}}(r, z) + \tilde{\boldsymbol{v}}(t, r, z),$$
$$p(t, r, z) = \bar{p}(r, z) + \tilde{p}(t, r, z),$$

where $\tilde{\boldsymbol{v}}$ and $\tilde{p}$ are small perturbation quantities.

The boundary conditions (u, v, w are radial, tangential and axial velocity components, respectively) are:

$$u\,(z = \{0, 1\},\ r,\ t) = w\,(z = \{0, 1\},\ r,\ t) = 0,$$
$$\text{and } \begin{cases} v\,(z = 0,\ r,\ t) = sr & \text{with } s \in [-1, 1[, \\ v\,(z = 1,\ r,\ t) = r, \end{cases}$$

By setting:

$$\bar{\boldsymbol{v}}(r, z) \begin{cases} \bar{u}(r, z) = rf'(z), \\ \bar{v}(r, z) = rg(z), \qquad \bar{p}(r, z) = r^2 h(z) + l(z), \\ \bar{w}(r, z) = -2f(z), \end{cases} \tag{2.1}$$

the steady Navier–Stokes equations are reduced to a system of well-known non-linear ordinary differential equations. Their solutions give the $f(z)$, $g(z)$, $h(z)$ and $l(z)$ functions.

The perturbation quantities are assumed to have normal-mode form:

$$\tilde{\boldsymbol{v}}(t, r, z) \begin{cases} \tilde{u} = \hat{u}(z) \exp[\mathrm{i}(kr - \sigma t)], \\ \tilde{v} = \hat{v}(z) \exp[\mathrm{i}(kr - \sigma t)], \qquad \tilde{p} = \hat{p}(z) \exp[\mathrm{i}(kr - \sigma t)], \\ \tilde{w} = \hat{w}(z) \exp[\mathrm{i}(kr - \sigma t)], \end{cases} \tag{2.2}$$

with $\sigma = \sigma_r + \mathrm{i}\sigma_i$ and $k = k_r + \mathrm{i}k_i$

Substituting (2.1) and (2.2) into the unsteady Navier–Stokes equations and linearizing with respect to the perturbation quantities $\tilde{u}$, $\tilde{v}$, $\tilde{w}$ and $\tilde{p}$, gives the system (2.3) with the parallel-flow approximation near r_p (the limitations implied are detailed in Lingwood 1995; Healey 2004). The parallel-flow assumption is usually introduced in the framework of flows that are strictly invariant with respect to streamwise translations. It has been applied to spatially developing flows by assuming that they remain pertinent locally at each streamwise station. It may be used for slowly spatially developing flows if the flow displays two distinct well-separated length scales, as justified by Huerre (2000). These concepts can be extended to the study of flows in confined geometry insofar as the disturbance wavelength is small in front of the cavity's radial extension and *a fortiori* for an infinite radial extension disk system. This assumption implies that the results are restricted to the local stability characteristics of the flow.
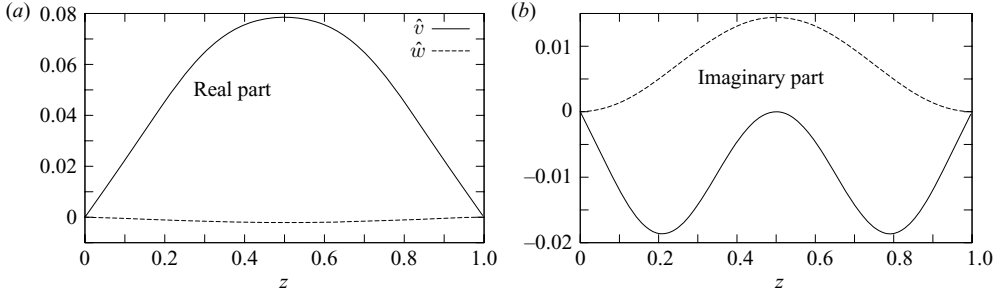
FIGURE 1. Profiles of (a) real and (b) imaginary parts of $\hat{v}$ and $\hat{w}$ for $s = -1$, $Re = 20$; $k_{rc} = 2.552$, $T_c = 2.66$ and $r_{pc} = 12.05$.
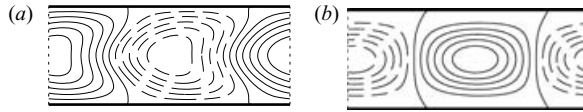

FIGURE 2. Instantaneous contours of (a) the real part of $\tilde{v}$ and (b) streamfunction $\tilde{\psi}$, over one wavelength for $s = -1$, $Re = 20$; $k_{rc} = 2.552$, $T_c = 2.66$ and $r_{pc} = 12.05$.

The system to be solved is written:

$$
\left\{
\begin{aligned}
&-i\sigma\hat{u} + ikf'\hat{u}r_p + \hat{u}f' - 2f\hat{u}' + r_pf''\hat{w} - 2g\hat{v} = -ik\hat{p} + \frac{1}{Re}\left[-k^2\hat{u} + \frac{ik\hat{u}}{r_p} - \frac{\hat{u}}{r_p^2} + \hat{u}''\right], \\
&\hspace{11cm} (2.3a) \\
&-i\sigma\hat{v} + ikf'\hat{v}r_p + g\hat{u} - 2f\hat{v}' + g'r_p\hat{w} + f'\hat{v} + g\hat{u} = \frac{1}{Re}\left[-k^2\hat{v} + \frac{ik\hat{v}}{r_p} - \frac{\hat{v}}{r_p^2} + \hat{v}''\right], \\
&\hspace{11cm} (2.3b) \\
&-i\sigma\hat{w} + ikf'\hat{w}r_p - 2f\hat{w}' - 2f'\hat{w} = -\hat{p}' + \frac{1}{Re}\left[-k^2\hat{w} + \frac{ik\hat{w}}{r_p} + \hat{w}''\right], \quad (2.3c) \\
&\hspace{4cm} \hat{u}\left(ik + \frac{1}{r_p}\right) + \hat{w}' = 0, \hspace{4cm} (2.3d)
\end{aligned}
\right.
$$

Boundary conditions:
$$\hat{u}(z = \{0, 1\}) = \hat{v}(z = \{0, 1\}) = \hat{w}(z = \{0, 1\}) = 0,$$

The elimination of the pressure $\hat{p}$ and the use of the continuity equation (equation (2.3d)) lead to a system of linear equations whose eigenfunctions are $\hat{v}$ and $\hat{w}$. The solution of this system for the parameter values considered gives the characteristics of the modes which destabilize the basic flow $\{\bar{v}(r, z), \bar{p}(r, z)\}$.

2.1. Temporal stability $(k_i = 0)$

For each Re and s value, the lowest r_{pc} value of r_p for which an unstable mode appears, characterized by a pair (k_r, σ) with $\text{Im}(\sigma) = \sigma_i = 0$, was investigated. Figure 1 shows the real and imaginary parts of $\hat{v}$ and $\hat{w}$ corresponding to the onset of the unstable mode for the rotation ratio $s = -1$. For this particular case, for all Reynolds numbers studied ($Re \leqslant 50$), there are disturbances, reflection-symmetric in the plane $z = 0.5$ for $\hat{v}$ and $\hat{w}$, which destabilize the basic flow. The disturbances $\tilde{v}$ and $\tilde{p}$ appear as centrifugal travelling waves. For instance, for $s = -1$ and $Re = 20$, the basic flow is stable for $r < r_{pc} = 12.05$. At this r_{pc} threshold value, the most unstable mode has period $T_c = 2.66$ and wavenumber $k_{rc} = 2.552$, which corresponds to a wavelength $\lambda_c = \lambda_c^*/e^* = 2.46$. For this particular case ($s = -1$, $Re = 20$), figure 2 shows the contours of $\tilde{v}$ and $\tilde{\psi}$ at a

Re	r_{pc}	k_{rc}	T_c	$\lambda_c = \lambda_c^*/e^*$
3	341.36	2.252	0.540	2.79
5	125.66	2.270	0.885	2.77
6	88.58	2.282	1.051	2.75
7	66.24	2.296	1.211	2.74
8	51.73	2.312	1.364	2.72
9	41.79	2.326	1.512	2.70
10	34.68	2.346	1.652	2.68
12	25.42	2.384	1.911	2.64
15	17.87	2.448	2.244	2.57
20	12.05	2.552	2.659	2.46
25	9.43	2.646	2.922	2.38
30	8.07	2.710	3.065	2.32
40	6.86	2.764	3.118	2.27
50	6.44	2.746	3.020	2.29

TABLE 1. Critical radius r_{pc} and characteristics of the first unstable mode between two coaxial exactly counter-rotating disks ($s = -1$) as a function of the Reynolds number.
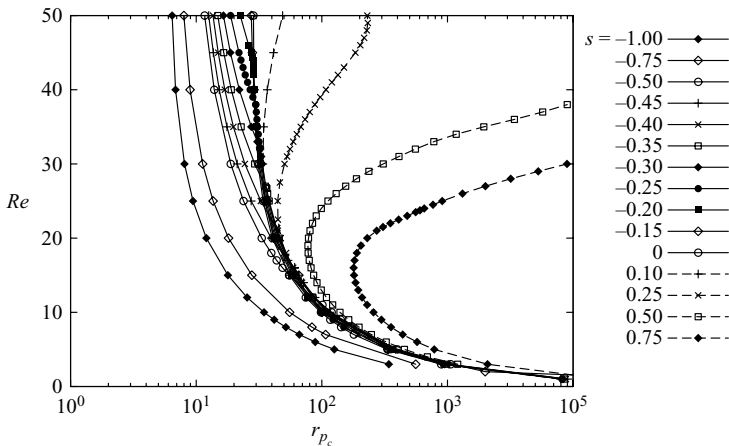
FIGURE 3. Neutral stability curves ($\sigma_i = 0$). Local critical radius r_{pc} as a function of Reynolds number Re for different rotation ratios s.

given time. Table 1 gives the characteristics and critical radius r_{pc} for the first unstable mode as a function of the Reynolds number, for exactly counter-rotating disks $s = -1$.

For the $s \neq -1$ values, the spatial distribution of $\hat{u}$, $\hat{v}$ and $\hat{w}$ ceases to be as simple, but the first unstable modes are always centrifugal travelling waves. There is generally one mode which destabilizes the basic flow first, but for certain values of Re and s, two unstable modes (characterized by two different values of k_r and σ_r) appear for the same critical value r_{pc}; this particular case will be detailed further.

The neutral stability curves are presented in figure 3. The critical local radius r_{pc} is plotted as a function of Re for different values of the rotation ratio s. For the range of Reynolds numbers studied here ($Re \leqslant 50$), the destabilization of the basic flow always occurs by the intermediary of a centrifugal wave for which the wavenumber k_{rc} varies with the Re and s values. These curves of neutral stability show behaviours which differ greatly depending on the value of the rotation ratio s.

Figures 4, 5 and 6 complete the description of the instabilities by representing the evolution of the critical wavenumber k_{rc} as a function of Re. The disturbances can then be classified into three families.
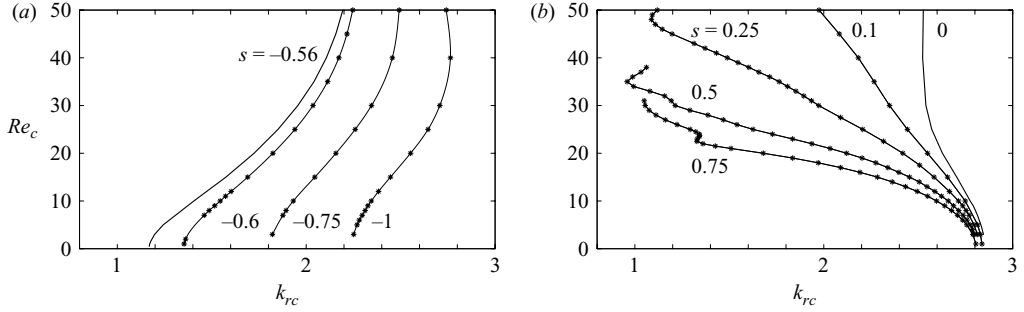
FIGURE 4. Neutral stability curves ($\sigma_i = 0$). Critical Reynolds number Re plotted against the critical wavenumber k_{rc} for different rotation ratio families (a) $s \in [-1, -0.56]$ and (b) $s \in [0, 0.75]$.
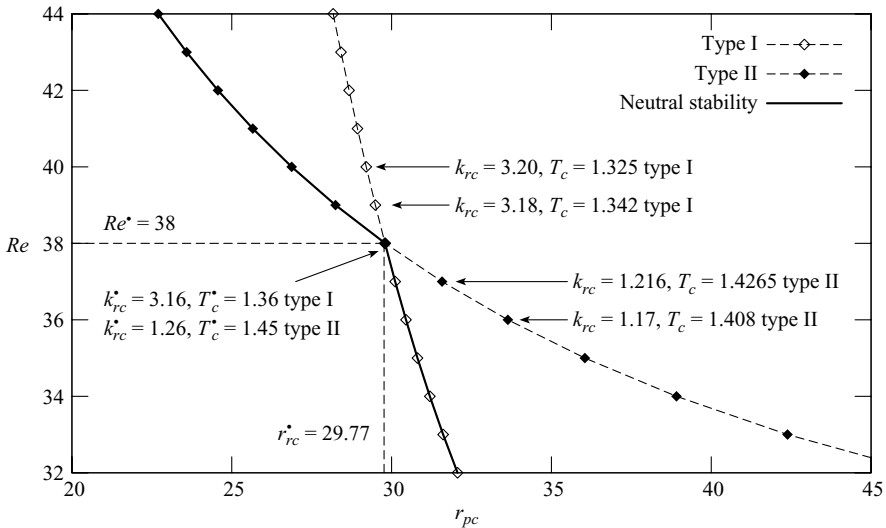

FIGURE 5. Neutral stability curves ($\sigma_i = 0$). Critical Reynolds number Re plotted against the critical radius r_{pc} for $s = -0.25$.

When the disks are strongly counter-rotating (i.e. $s \in [-1, -0.56]$; cf. figure 4a) the basic flow is destabilized by a disturbance with a critical wavenumber which evolves slightly as Re increases, but increases when s tends towards -1.

When the disks are co-rotating (i.e. $s \in [0, 1]$; cf. figure 4b) the critical wavenumber of the disturbance does not always evolve monotonically with Re. In the boundary case $s = 0$, the critical wavenumber varies slightly, passing from $k_{rc} = 2.84$ with $Re = 3$, to $k_{rc} = 2.52$ with $Re = 50$. The disturbance's characteristics are similar (same r_{pc} and k_{rc}) to those described by San'kov & Smirnov (1992) for low Re values. On the other hand, for higher values of the rotation ratio, the evolution of k_{rc} with Re is much more noticeable (e.g. $k_{rc} \in [0.96, 2.8]$ for $s = 0.5$) and beyond a particular value of Re, the evolution of k_{rc} ceases to be monotonic. This change of behaviour could be attributed to the onset of boundary layers on the disks.

For intermediate values of the rotation ratio (i.e. $-0.56 < s < 0$), the evolution of the critical wavenumber with the parameters Re and s is appreciably more complicated. Indeed, as previously mentioned, there is thus for each value of $s \in]-0.56, 0[$, a
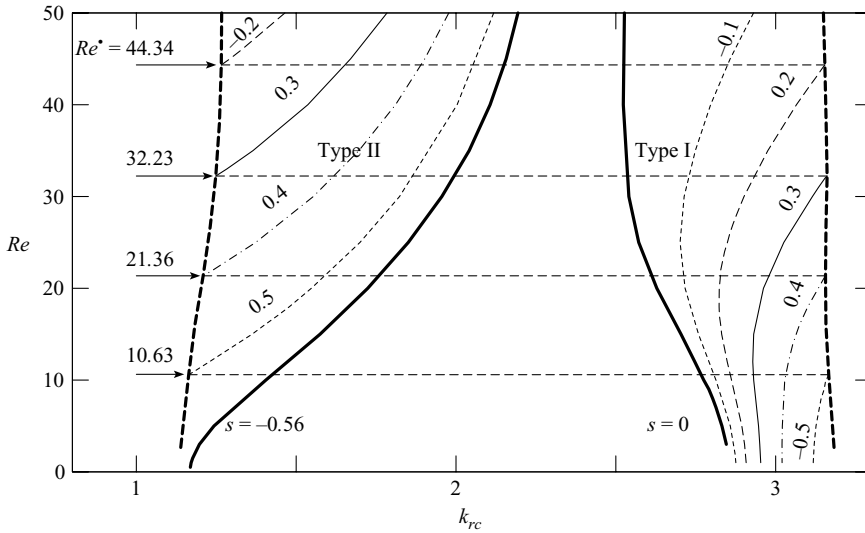
FIGURE 6. Neutral stability curves ($\sigma_i = 0$). Critical Reynolds number Re plotted against the critical wavenumber k_{rc} for $s \in]-0.56, 0[$.

s	$r_{pc}^\bullet$	$Re^\bullet$	Type I		Type II	
			$k_{rc}^\bullet$	$T_c^\bullet$	$k_{rc}^\bullet$	$T_c^\bullet$
−0.15	27.295	51.69	3.148	1.1804	1.2672	1.3702
−0.20	28.285	44.34	3.154	1.2766	1.2658	1.3712
−0.25	29.765	38.00	3.158	1.3597	1.2600	1.4448
−0.30	32.215	32.23	3.162	1.4555	1.2486	1.4133
−0.35	36.360	26.72	3.158	1.5429	1.2310	1.4400
−0.40	44.030	21.36	3.156	1.5511	1.2090	1.3462
−0.45	60.700	16.00	3.158	1.4457	1.1832	1.2624
−0.50	109.405	10.63	3.166	1.3052	1.1640	0.9572
−0.55	1397.750	2.66	3.182	0.3819	1.1380	0.2921

TABLE 2. Particular values $Re^\bullet$, for which two unstable modes appear with different wavenumbers for the same local radius $r_{pc}^\bullet$

particular value $Re^\bullet(s)$ for which two unstable modes appear for the same $r_{pc}^\bullet$ value of the local radius. These modes (cf. figure 6) are characterized in particular by very different $k_{rc}^\bullet$ values. Type I has a relatively large wavenumber $k_{rc}^\bullet$, about 3.2, whereas type II has a much smaller wavenumber, about 1.2. The main results are indicated in table 2 for the s values concerned. It can be seen that there are few differences between the critical periods $T_c^\bullet$ of both types, except for the low $Re^\bullet$ values. As an example, figure 5 details the loss of stability of the basic flow in the case $s = -0.25$. For the case considered, $Re^\bullet(s = -0.25) = 38.00$ and $r_{pc}^\bullet = 29.8$ (cf. table 2), for each value of $Re < Re^\bullet$, there is a value $r_{pc}^I(Re) > r_{pc}^\bullet$, for which the basic flow is initially destabilized by a mode of type I. For instance, for $Re = 36$, $r_{pc}^I = 30.45$, $k_{rc}^I = 3.116$; for $Re = 34$, $r_{pc}^I = 31.195$, $k_{rc}^I = 3.078$. The flow is also destabilized by a type II mode, but this occurs for a value $r_{pc}^{II} > r_{pc}^I$.

For $Re = Re^\bullet = 38.0$, both modes I and II destabilize the basic flow at $r_{pc}^I = r_{pc}^{II} = r_{pc}^\bullet$. For $Re > Re^\bullet$, there is initial destabilization by a type II mode, which occurs with a value r_{pc}^{II} lower than the r_{pc}^I value for which the type I mode is destabilized. For instance, for $Re = 39$, $r_{pc}^{II} = 28.245$, $k_{rc}^{II} = 1.302$; $r_{pc}^I = 29.495$, $k_{rc}^I = 3.18$; for $Re = 40$, $r_{pc}^{II} = 26.875$, $k_{rc}^{II} = 1.34$; $r_{pc}^I = 29.205$, $k_{rc}^I = 3.202$. Figure 6 shows all of the results for $-0.56 < s < 0$. For each of these s values, the process is the same as that described in detail above: for $Re < Re^\bullet(s)$, the flow is destabilized by a type I mode with a relatively large wavenumber (e.g. $k_{rc} = 3.12$ for $s = -0.5$ and $Re = 3$), then, as the Reynolds number increases until it reaches $Re^\bullet(s)$, the disturbance wavenumber evolves until reaching the particular value $k_{rc}^{\bullet I}$ (e.g. $k_{rc}^{\bullet I} = 3.166$, $Re^\bullet = 10.63$). For these same values of $Re^\bullet$ and $r_{pc}^\bullet$, a second disturbance (type II) appears with a lower wavenumber ($k_{rc}^{\bullet II} = 1.164$, $Re^\bullet = 10.63$). For $Re > Re^\bullet$, it is this second disturbance which first destabilizes the flow as r_p is increased outwards. All of the particular points $k_{rc}^{\bullet I}(Re^\bullet)$ and $k_{rc}^{\bullet II}(Re^\bullet)$ are indicated in thick dotted lines in figure 6.

Table 2 gives some parameter values for which two disturbances of different wavenumbers appear at the same local radius.

2.2. *Spatio-temporal stability* ($k_i \neq 0$)

As shown above, the von Kármán swirling flow between two infinite coaxial disks can become unstable from a critical fixed radius for a low Reynolds number ($Re \leqslant 50$). Lingwood (1995, 1996) showed that, in the case of the boundary layer over a disk rotating in otherwise still fluid, the flow becomes absolutely unstable beyond a certain radius. The wave packet which destabilizes the basic flow consists of two families of travelling waves. Taking into account similarities existing between the case investigated by Lingwood and the case examined here, the question of the nature of the instability (convectively unstable CI or absolutely unstable AI) highlighted in §2.1 arises. By examining the behaviour of disturbances with complex wavenumber ($k = k_r + \mathrm{i}k_i$ with $k_i \neq 0$) and by applying the Briggs–Bers criterion (cf. Huerre & Monkewitz 1990; Delbende, Chomaz & Huerre 1998) for the critical values $r_{pc}(Re)$, we found a saddle point corresponding to a pinching point of the two branches k^+ and k^- (according to the notations of the above-mentioned authors). The value of $\sigma_i^\star$ at this saddle point determines the nature CI or AI of the instability. However, for the critical values indicated §2.1, the values of $\sigma_i^\star$ are very slightly negative (cf. figure 7a: $\sigma_i^\star(Re = 25, s = -1, r_p = r_{pc} = 9.43) \approx -9.1 \times 10^{-5}$). The aim is thus to study the sensitivity of $\sigma_i^\star$ as a function of r_p: is there a change in the sign of $\sigma_i^\star$ for an $r_p^\star$ value slightly higher than r_{pc}?

By carrying out computations similar to those presented in figure 7(a), but for the value $r_p = 9.55$ (that is to say an increase of less than 2%), the value of $\sigma_i^\star(Re = 25, s = -1, r_p = r_{pc} = 9.55)$ became positive (cf. figure 7b): $\sigma_i^\star \approx 2.91 \times 10^{-4}$. Although this is not a systematic study of all $r_{pc}(Re, s)$ cases, the same type of result was found for the few cases treated. The flow is absolutely unstable locally and it is known (cf. Huerre & Monkewitz 1990) that this can lead to the onset of a global unstable mode. It thus seems that, for the values of $Re \leqslant 50$ considered, this conclusion can be generalized for all $s \in [-1, 1[$ values. Of course, for values much higher than r_{pc}, the present linear stability analysis is no longer valid and cannot give any indication, because of the usual nonlinear superposition of all of the unstable modes.

An interesting case is that corresponding to $s \in]-0.56, 0[$, for which, for an identical Re value there are two modes which destabilize the basic flow with the same $r_{pc}^\bullet$. Figures 7(c) and 7(d) present examples of results obtained for $Re^\bullet = 38$ and
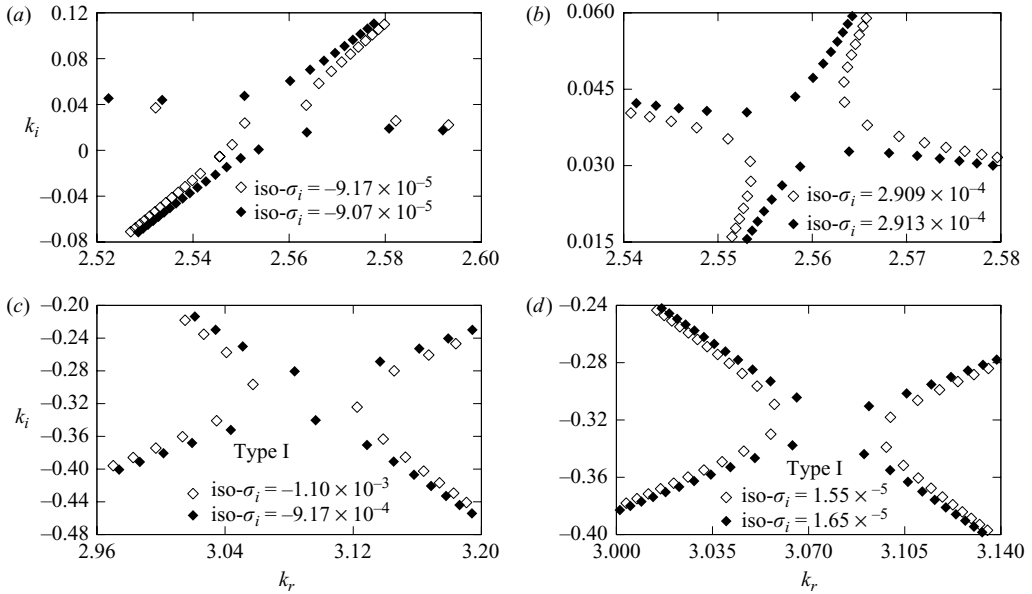
FIGURE 7. Contours of σ_i in the complex (k_r, k_i) plane. Locus of the saddle point $\sigma_i^\star$ with $Re = 25$ and $s = -1$. (a) $\sigma_i^\star(r_{pc} = 9.43) \approx -9.1 \times 10^{-5} < 0$. The flow is CI. (b) $\sigma_i^\star(r_p = 9.55) \approx 2.91 \times 10^{-4} > 0$. The flow is AI. Locus of the saddle point $\sigma_i^\star$ with $Re^\star = 38$ and $s = -0.25$. (c) $\sigma_i^\star(r_{pc} = 29.77) \approx -1 \times 10^3 < 0$. The flow is CI. (d) $\sigma_i^\star(r_p = 30.5) \approx 1.6 \times 10^{-5} > 0$. The flow is AI.

$s = -0.25$. The preceding temporal stability study showed that for these parameter values, the basic flow is destabilized from $r_{pc}^\bullet = 29.77$ by two modes (Types I and II) with wavenumbers $k_r^{\bullet I} = 3.158$ and $k_r^{\bullet II} = 1.26$, respectively. Figure 7(c) shows that for $r_{pc}^\bullet = 29.77$, the flow is convectively unstable ($\sigma_i^\star < 0$) with respect to the type I disturbance (the wavenumber $k_r^\bullet$ corresponds to that given by the temporal analysis for type I instabilities). Figure 7(d), on the other hand, shows that starting from $r_p = 30.5$, the flow becomes absolutely unstable ($\sigma_i^\star > 0$) with respect to the same type I disturbance. The local radius of transition AI/CI is thus very close, less than half a wavelength, to the local critical radius $r_{pc} = 29.77$ from which the von Kármán swirling flow becomes unstable. On the other hand, the basic flow is convectively unstable only with respect to type II disturbances.

3. Cavity flow

It remains to be determined whether the loss of stability of the self-similar solutions calculated above subsists in the case of a finite physical problem, i.e. for a realistic shrouded disk system of finite radial extension. More precisely, the destabilization of the self-similar solutions is compared here with the conditions of appearance of unsteady flows in a cavity consisting of two coaxial disks enclosed in a stationary sidewall.

3.1. *Implementation*

The integration of the axisymmetric non-stationary Navier–Stokes equations was carried out by means of a pseudospectral computational method of collocation, associating spatial approximations in the form of a truncated series of Chebyshev
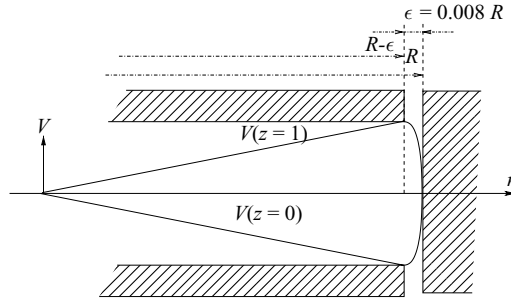
FIGURE 8. Sketch of the tangential velocity variation between the two rotating disks and the fixed sidewall for $s = -1$. The connection of the velocity from the rotating disks to the zero velocity at $r = R$ was carried out by continuity through a small radial gap ϵ.

polynomials with a temporal discretization by second-order finite differences. This scheme showed, in similar conditions, its aptitude to highlight instabilities in cavity flows (see Cousin-Rittemard *et al.* 1998, 1999). In addition to the three parameters on which the flow depends (Re, s, R), it is necessary to examine the way in which the tangential velocity decreases to zero from the rotating disk to the fixed sidewall through a small radial gap ϵ at $r = R$. It was first imposed that the tangential velocity vary linearly in z between the higher and the lower disk $(\epsilon = 0)$. The boundary condition of the tangential component is then:

$$\forall z \in [0, 1] \quad v(R, z) = (1 - s)Rz + sR, \tag{3.1}$$

Then, in a more realistic way, the connection of the velocity from the rotating disks to the zero velocity at $r = R$ was carried out by continuity through a small radial gap ϵ (cf. figure 8). The size of this space was taken as equal to $\epsilon = 0.008R$ in agreement with the value fixed in the experimental device described further and corresponding to the particular case $R = 15$. These conditions are written:

$$\forall t \begin{cases} \text{at } r = R; \quad z \in [0, 1]; \quad v = 0, \\ \text{at } r = R - \epsilon; \quad \begin{cases} z = 0; \quad v = s(R - \epsilon) \quad \dfrac{\partial v}{\partial r} = s, \\ z = 1; \quad v = R - \epsilon \quad \dfrac{\partial v}{\partial r} = 1, \end{cases} \end{cases} \tag{3.2}$$

A suitable description of this region requires an increased radial resolution, denser near the periphery. The Gauss–Lobatto grid used is well suited since it generates an increased density of points in the boundary regions. Practically no difference was observed in the critical values of the parameters or in the corresponding flow structures.

3.2. Results

Several values of the aspect ratio were studied, but mainly the results relating to the aspect ratio $R = 15$ will be presented.

3.2.1. A priori estimation of the critical Reynolds number in a cavity

In the case of infinite disks, previous results show that, for fixed s, there is a relation $Re(r_{pc})$. For a cavity of given aspect ratio, the critical value of Re can be estimated by comparing r_{pc} with R. It seems clear that, for fixed Re, instability cannot be observed if $r_{pc} > R$ (by assuming that the destabilization mechanism of the flow is the same in a cavity and between infinite disks). For example, for $s = -1$, the self-similar solution threshold $Re_c^{(a)}(r_{pc} = R = 15)$, is $Re_c^{(a)} \approx 17.5$.

s	-1	-0.95	-0.9	-0.85	-0.8	-0.75	-0.7
Re	20	20	20	20	25	30	33
r_l/R	0.85	0.75	0.70	0.67	0.64	0.63	0.61

TABLE 3. Estimation of the region $r \leqslant r_l$ where the self-similar solutions represent correctly the flow in a cavity of large aspect ratio ($R = 15$). The local radius r_l indicates the radial position from which the maximum value of the axial velocity w deviates by more than 5% compared to the maximum value of w given by the self-similar solutions. Beyond this radius the self-similar solutions are no longer valid in the cavity. These values correspond to a steady flow, just before the unsteady onset.
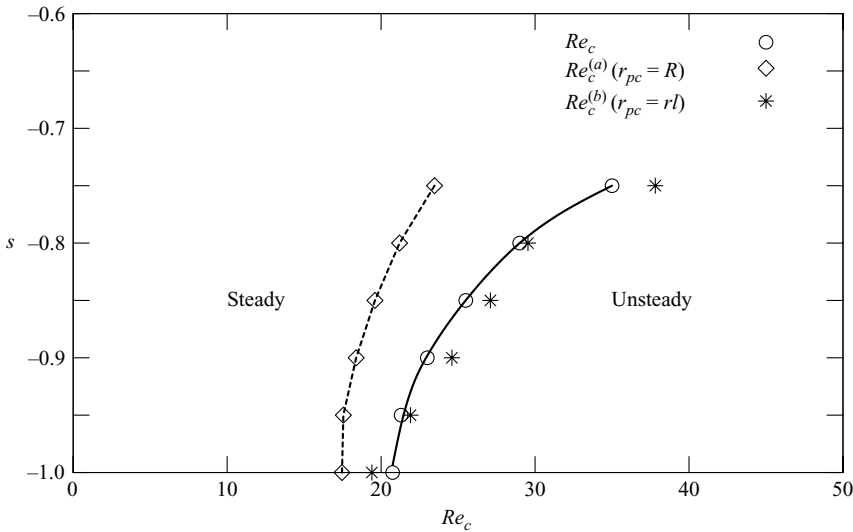
FIGURE 9. Neutral stability curves $s(Re)$ of von Kármán self-similar solutions (---) and in an $R = 15$ aspect ratio cavity (—).

The numerical integrations carried out in a cavity of aspect ratio $R = 15$ confirm that for $Re = 17.5$ the flow remains steady, whatever the conditions imposed on the sidewall. The comparison between the steady flow field velocity computed in the cavity and the velocity flow field given by the self-similar solutions shows a very good agreement in the entire cavity, except in a peripheral region whose radial extent $r_l \in]0, R]$ varies with s and Re (cf. table 3).

If, as appears probable, destabilization in the cavity should occur at the radius r_l, the curves plotted in figure 3 make it possible to deduce the critical Re value; for example, in the particular case $s = -1$, $R = 15$: $Re_c^{(b)}(r_{pc} = r_l = 12.75) \approx 19.4$. Using the same method for $s \in [-0.95, -0.7]$, the values $Re_c^{(a)}$ and $Re_c^{(b)}$ can be deduced and are represented in figure 9.

In a cavity, the instability threshold is detected by flow behaviour observation at several points located in the cavity mid-plane ($z = 0.5$) and at various r values. The level of the disturbances is an increasing function of r until the vicinity of the sidewall ($r \approx r_l$), where it falls rapidly to zero.

For given s and R, by measuring the maximum disturbance level as a function of Re, the critical value Re_c corresponding to the destabilization of the basic flow can be detected. This loss of stability occurs via a supercritical Hopf bifurcation.
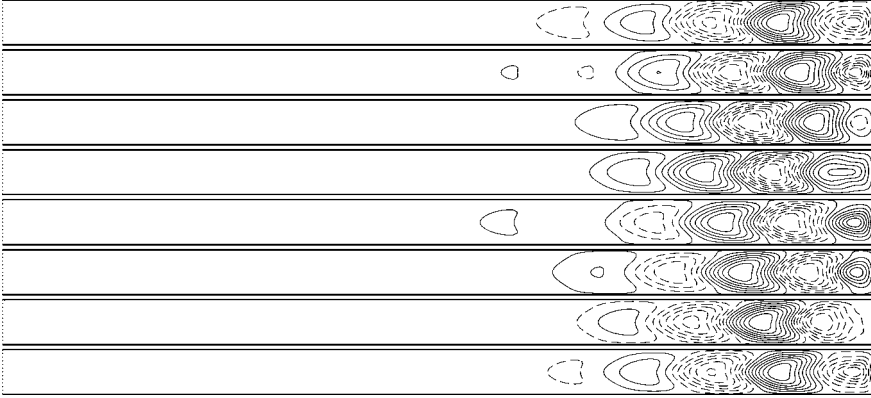
FIGURE 10. Structure in the meridional plane of the tangential velocity disturbance in a cavity of aspect ratio $R = 15$; contours of $\tilde{v}$ over a period (the time increases from top to bottom with an increment of 0.38) for $Re = 21$ and $s = -1$. The axis is on the left and the sidewall on the right of each figure.

Near criticality, the square of the disturbance level varies linearly with Re. This property makes it possible to calculate precisely the critical Reynolds number Re_c by calculating the disturbance level for Re values very slightly above Re_c, this critical value is obtained by extrapolation. For the flow studied here, this vicinity is restricted because of the very strong increase in the instability level with Re. The critical Re_c values thus obtained in the cavity are also plotted in figure 9 and are represented by ($\circ$). A good coincidence between the $Re_c^{(b)}$ values and those of the cavity can be seen; this shows that the loss of stability of cavity flows (for sufficiently large R) is predicted well by the temporal linear stability analysis of the self-similar solutions (disks of infinite radial extent), provided that the stabilizing effect of the sidewall is taken into account. In addition, figure 3 shows that, for all s, the flow in cavities of small aspect ratio R is not destabilized by axisymmetric modes (the critical radius r_{pc} being higher than the cavity length R). Computations for cavities of different aspect ratios showed that the lower limit of axisymmetric instabilities onset may be estimated at $R \approx 10.3$. This is in agreement with reports that for relatively small aspect ratios the thresholds of axisymmetric instabilities are higher than those of non-axisymmetric modes.

3.2.2. Structure and properties of instabilities in cavity

At the loss of stability of the basic flow, the disturbances consist of centrifugal travelling waves, as described in §2.1. As an example, figure 10 shows the temporal evolution over one period of the disturbance $\tilde{v}(t, r, z)$ for $R = 15$, $Re = 21$ and $s = -1$. Except in the vicinity of the sidewall, it can be seen that the instability structure in the cavity is identical to that of the self-similar solutions (cf. figure 2). In the same way, excellent coincidences can be seen between the critical periods and wavelengths of the cavity instabilities and the instabilities between disks of infinite extent ($s = -1$, $R = 15$, $Re = 21 : T_c^{cav} = 2.64$, $T_c^{R\infty} = 2.62$; $\lambda_c^{cav} = 2.5$, $\lambda_c^{R\infty} = 2.44$).

However, there is an essential difference between computations in cavity and the results of §2.1: the disturbance level is a function of r in the case of the cavity. Figure 11(a) shows the dependence of $\tilde{v}(t, r, z = 0.5)$ on r for $R = 15$, $s = -1$, $Re = 21$, as well as the associated envelope of its temporal fluctuations. It is seen that the disturbance level tends very rapidly towards zero when $r \to 0$, but a thorough examination of this behaviour reveals that the disturbance level decreases in a very
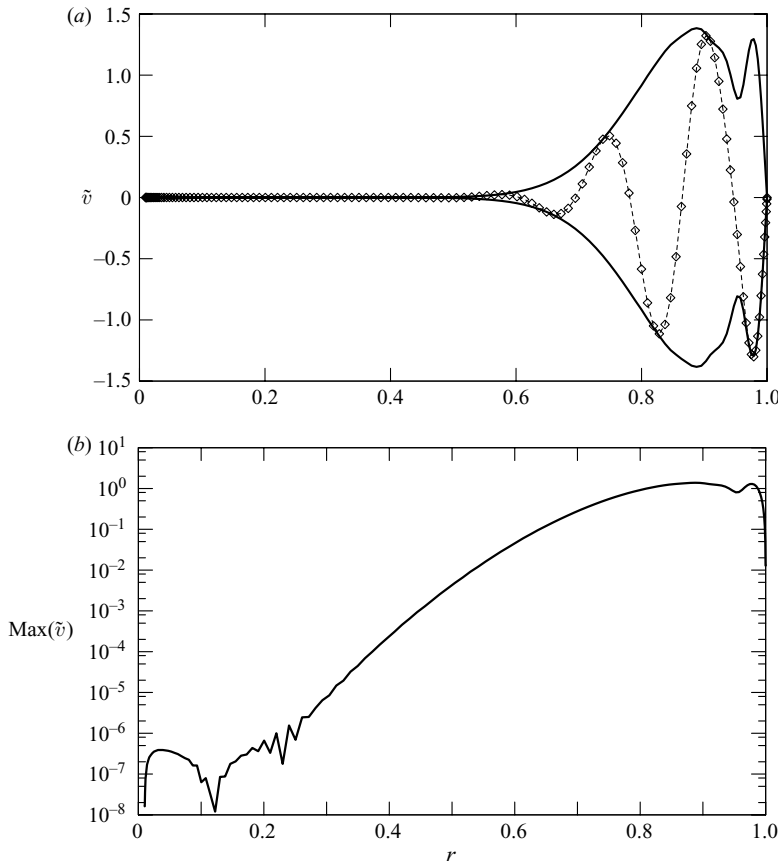
FIGURE 11. Level of the tangential component of the instability $\tilde{v}(r, z = 0.5, t)$ as a function of radius for $R = 15$, $s = -1$ and $Re = 21$. (*a*) Instantaneous evolution of $\bar{v}(t)(\cdots\diamond\cdots)$ and the associated envelope of its temporal fluctuations. (*b*) Maximum of $\bar{v}(t)$ temporal fluctuations.

distinctive way (cf. figure 11*b*). This characteristic is connected with results previously mentioned in §2.2: the presence of an absolute instability region very close to the critical radius where the destabilization of the basic flow occurs has been shown. This consolidates the idea that instability in a cavity is due to a global unstable mode (cf. Huerre & Monkewitz 1990), so that the destabilization of an axisymmetric basic flow in a cavity of large aspect ratio can be considered in the following way for $R \gg 1$ and a given s value.

  (i) As long as $Re < Re_c^{(b)}(r_l)$, the unsteady disturbances are destroyed with time; the flow is stable.

  (ii) For $Re = Re_c \approx Re_c^{(b)}(r_l)$, even an infinitesimal disturbance at $r = r_l$, will generate a global mode filling the whole cavity.

3.2.3. *Stability diagram ($R = 15$).*

  The stability diagram in figure 12 shows the values (Re_c, s) for which the axisymmetric basic flow loses its stability with respect to axisymmetric disturbances. The flow then becomes unsteady for a wider range of Re values as s approaches -1 (the case of exactly counter-rotating disks). For the lowest Re_c values, the branch of the diagram reproduces that indicated in figure 9 with ($\circ$). Because of the stabilizing effect
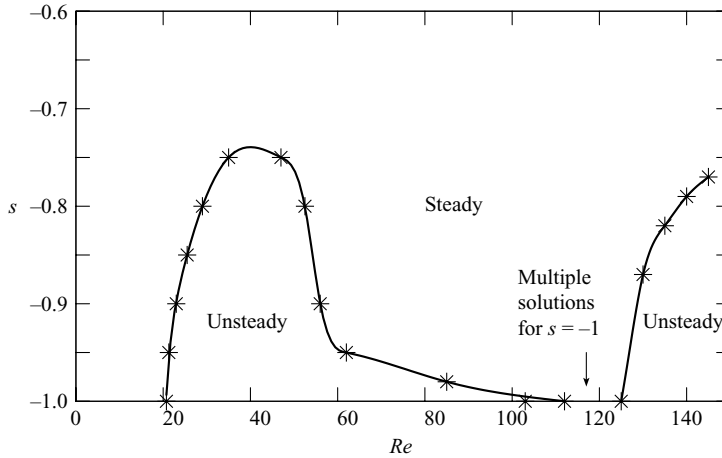
FIGURE 12. Stability diagram for axisymmetric modes in cavity ($R = 15$).

of the sidewall and since a decreasing proportion of the flow resembles the self-similar solutions in the cavity as s and Re increase (cf. table 3), it can be seen that the basic flow remains stable for all Re for $-0.74 \leqslant s \leqslant 0$ and that there is a return to steady flow for $-1 \leqslant s \leqslant -0.74$ as Re increases. However, this return to steady flow occurs in a different way, as a function of the s value.

For $s \in]-1, -0.74]$, the steady solution is of a similar type on both sides of the area delimiting the onset of the unsteady solution. These solutions belong to the branch described by Szeto (1978) for the similar problem between infinite disks. The destabilization, and the return to steady flow as the Reynolds number increases, occur via two supercritical Hopf bifurcations. In contrast, if $s = -1$, the evolution is much more complicated, as will be detailed further. First, there is a supercritical Hopf bifurcation at $Re = 20.7$, which leads to transition from the steady solution of Stewartson (1953) (symmetric with regard to the midplane between the disks for u and antisymmetric for v and w) to a periodic solution (which preserves, on average, the basic flow properties), and secondly, the return to a steady solution which occurs by means of a subcritical bifurcation. This leads to two steady solutions, having lost the symmetry properties of the initial stable solution.

These two steady solutions then become unstable for $Re = 125.2$. The new solution appears as quasi-stationary waves in the whole cavity where the velocity and pressure fields oscillate periodically at each point. As s tends towards zero, this area of instability joins that already highlighted in the rotor–stator configuration and which corresponds to a boundary-layer-type instability (cf. Jarre, Le Gal & Chauve 1991, 1996; Schouveiler *et al.* 1998, 2001; Gauthier *et al.* 1999). The passage from one type of instability to the other, as s increases from -1 to 0, is still not completely elucidated. The remainder of this paper is restricted to the description of the main characteristics of the first unsteady area in figure 12 (i.e. up to $Re = 120$), with particular attention to the $s = -1$ case which corresponds to the most complex situation.

3.2.4. *Unsteady stable solutions ($R = 15$, $s = -1$)*

Figure 13 shows the amplitude of the tangential velocity component fluctuations v, monitored at ($r = 0.7$, $z = 0.5$), as a function of Re. As already observed for low
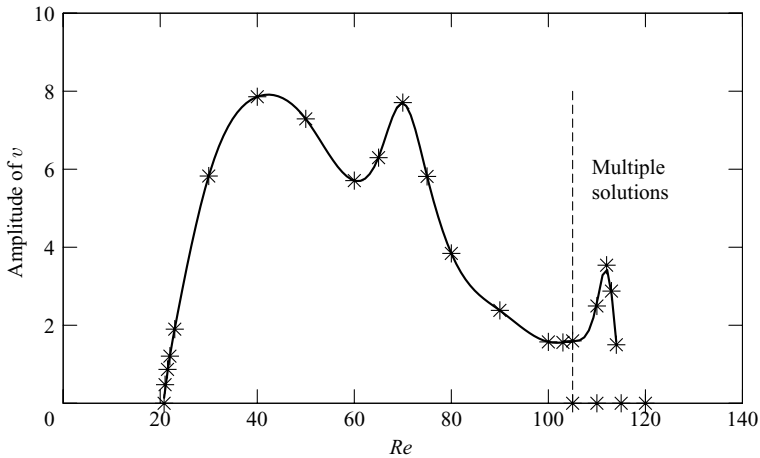
FIGURE 13. Amplitude of the tangential velocity component $v(t)$ as a function of Re at $(r = 0.7, z = 0.5)$ for $R = 15$ and $s = -1$.

Re values, the axisymmetric basic flow remains stable with respect to axisymmetric disturbances, in agreement with the results of Szeto (1978) for the steady self-similar solutions. At $Re_c = 20.7$, the basic flow becomes unstable and the associated bifurcation is a Hopf supercritical as previously mentioned. For $20.7 \leqslant Re \leqslant 50$, the disturbance has the same structure (centrifugal travelling waves with a basic period T_0 and a phase velocity increasing with Re). The fluctuation amplitude also increases with Re and passes through a maximum in the vicinity of $Re = 40$, at which point $v(t)(r = 0.7, z = 0.5)$ reaches 75% of the tangential velocity of the disk at the same radius.

From $Re = 65$, significant modifications appear in the spatio-temporal evolution of the flow. When Re reaches 70, the travelling waves are affected by deformations in almost the whole field, with dislocations near the periphery. In the vicinity of $Re = 100$, the level of the disturbance is minimal. There is almost no further propagation, except by means of dislocations near the sidewall. From $Re = 111$, the evolution of v at the monitored point is similar to a periodic signal and the level of the disturbance becomes maximum for Re close to 112. Beyond this value, a rapid decrease with Re can be observed in the level of the disturbance. Moreover a qualitative change could be observed in the density power spectrum evolution of the time-dependant solution with the occurrence of period-doubling oscillations. The spectrum shows the presence of an $f_0/2$ subharmonic and several linear combinations $mf_0 + nf_0/2$ ($f_0 = 1/T_0$ is of the order of 0.56). It can thus be conjectured that the structure's loss of stability is achieved by a subcritical bifurcation with hysteresis.

3.2.5. *Return to stationarity ($R = 15, s = -1$).*

When $Re = 114$, a sudden change takes place, which leads to a steady solution after a very long transient evolution (figure 14). In fact, two steady solutions can be obtained. These two solutions $S_1[u_1(r, z), v_1(r, z), w_1(r, z)]$ and $S_2[u_2(r, z), v_2(r, z), w_2(r, z)]$ are related by simultaneous reflection in tangential θ and in axial z-coordinates.

These solutions are similar to those found by Szeto (1978) for $Re \geqslant 119.4$ in the case of disks of infinite radial extent. As Re increases, these solutions remain stable until $Re = 125.2$ where a Hopf bifurcation leads to an unsteady solution.
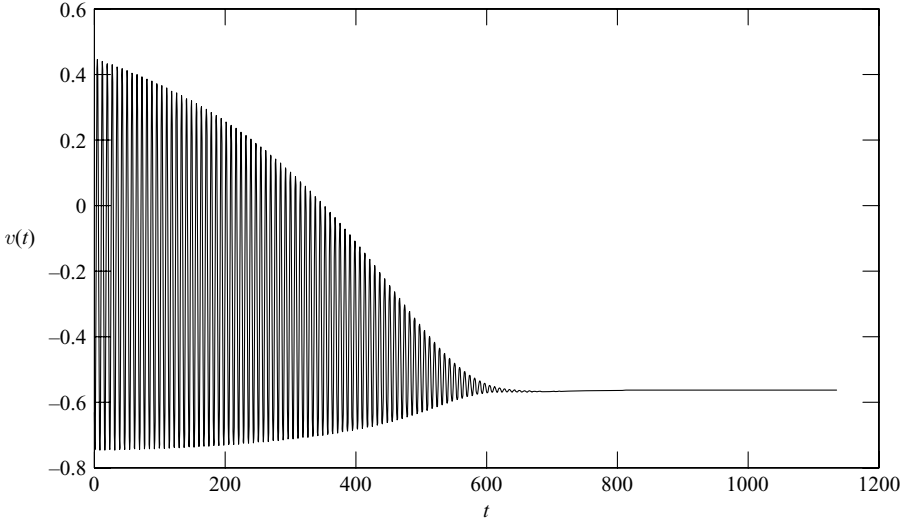
FIGURE 14. Time series of the tangential velocity component $v(t)$ at $(r = 0.7, z = 0.5)$ for $R = 15$, $s = -1$ and $Re = 114$. Final steady solution.
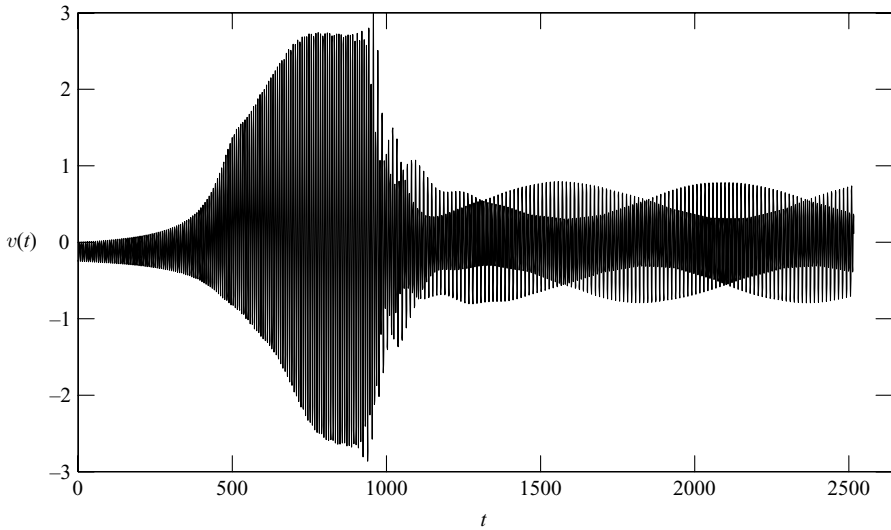

FIGURE 15. Time series of the tangential velocity component $v(t)$ at $(r = 0.7, z = 0.5)$ for $R = 15$, $s = -1$ and $Re = 104.5$. Final unsteady solution.

3.2.6. *Nature of the bifurcation between $Re = 113.8$ and $Re = 114$*

From one or the other of the two solutions obtained for $Re \geqslant 114$, decreasing Re leads to a solution which remains steady. Obtaining such solutions is possible while decreasing Re to 105. On the basis of the solution thus obtained for $Re = 105$ as initial solution, and by carrying out integration for $Re = 104.5$, the corresponding unsteady solution is found after very long transients (cf. figure 15). The signal is then quasi-periodic with a spectrum showing a few characteristic frequencies which can all result from two basic frequencies: $f_0 = 0.643$ ($T_0 = 1.554$) and $f_l = 0.007$ ($T_l = 139$). The most energetic frequencies are f_0 and $(f_0 + f_l)/2$, the latter being very close to
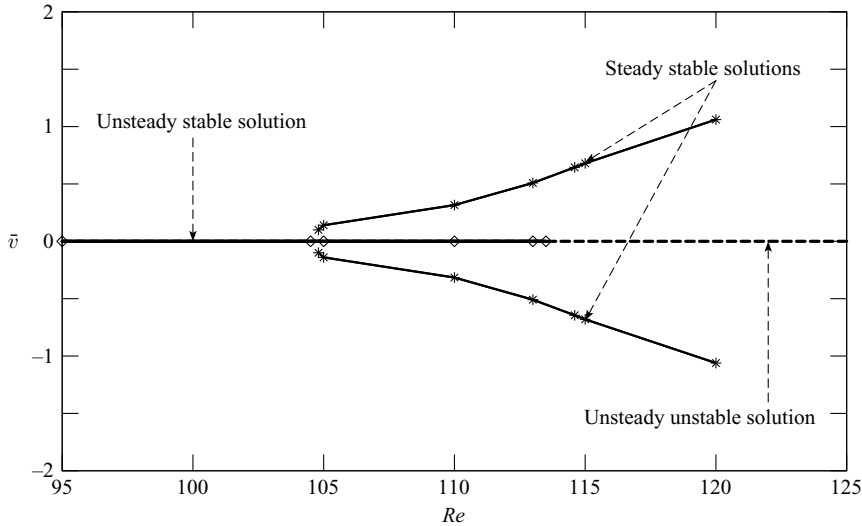
FIGURE 16. Bifurcation diagram. Mean value of the tangential velocity component $\bar{v}$ as a function of Re at $(r = 0.7, z = 0.5)$ for $R = 15$, $s = -1$.
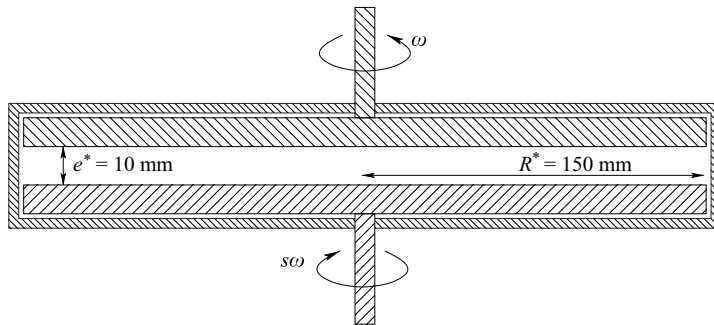

FIGURE 17. Experimental device.

the subharmonic $f_0/2$. There is thus, between $Re = 105$ and $Re = 113.8$, the possibility of obtaining three different stable solutions:

an unsteady solution which becomes unstable for $Re > 113.8$;

two steady solutions with characteristics as described above.

This comes from the subcritical character of the associated bifurcation which is shown in figure 16 where the average value $\bar{v}$ of the tangential component at the monitored point is plotted for each solution as a function of Re.

3.3. *Experimental results in a cavity with $R = 15$ aspect ratio*

The existence of the primary bifurcation, indicating the loss of stability of the basic flow and the onset of an unsteady disturbance, is investigated experimentally for the particular case, $s = -1$, $R = 15$. The working fluid is water of kinematic viscosity $\nu^* = 10^{-6}$ m^2 s^{-1} at 20 °C and the Reynolds number is controlled to within 2%. The experimental set-up (figure 17) consists of two coaxial glass disks, $R^* = 150$ mm radius and $e^* = 10$ mm gap width. Each disk is mounted on a vertical drive shaft which, through a system of waterproof ball bearings, can rotate inside an Altuglas housing

enclosure. Disks are driven independently of each other by electronically regulated electric motors.

Velocity measurements have been taken by means of a laser doppler velocimetry system. This consists mainly of a 35 mW He-Ne Laser (Spectra-Physic), an optical system with a Bragg cell and a front lens (300 mm focal length), and a signal processor (Dantec). A frequency shift is superposed by the Bragg cell onto one of the two beams to allow the measurement of very weak or reversing flows. Because of the characteristic time of the expected disturbance (the calculation indicated a dimensional period of about 10 s) it is necessary to sample data during a sufficiently long period, and particular care must be given to the quality of the seed particles. Because of the dioptric effect formed by the curved surfaces of the housing and also by the rotating disks, the optical beam access within the flow field is very limited. The tangential component was measured because it was easier to obtain. The probe measure was placed at $r = 12$ and $z = 0.42$. Figure 18 represents the evolution, as a function of time, of the tangential velocity component. Up to $Re = 22$, no characteristic frequency is released; only noise is visible on the figure owing to the difficulty in measuring very low velocity, about 1 mm s^{-1}. The mean value of the velocity is equal to that of the self-similar solutions. For $Re = 23$, the appearance of a periodic fluctuation of the velocity at the measuring probe can be clearly seen. It is difficult to measure the slight oscillation amplitude increases when the Reynolds number increases because of the noise on the signal. Oscillations cease to be mono-periodic from $Re = 25$, which can be attributed to the contamination of the zone in which the probe volume is situated by three-dimensional disturbances observed near the sidewall, which will be described further. Beyond $Re = 30$, the signal enriches by many frequencies and its fluctuations become more complicated, but the average value remains that given by self-similar solutions.

Visualizations of the flow have been obtained by laser sheets in horizontal and meridional planes. The light emitted by an argon laser (Spectra-Physics 2016) was transmitted by an optical multimode fibre to an optical system of light-sheet generation. The flow was seeded with particles of titanium dioxide (TiO$_2$), and photographed.

Visualizations in meridional planes have been found particularly difficult to obtain because of the strong tangential component of the main flow velocity. The length of time the particles stay in the illuminated zone is thus very short, preventing the recording of the trace of the perturbation sought in the visualization plane. To remedy this problem, the illuminated zone (≈ 3 mm) was widened so as to take into account axial and radial components of the particle paths. Visualizations in a plane parallel to the disks are easier to obtain. For $s = -1$, the axial and tangential components of the flow mean velocity are zero at $z = 0.5$, and thus the particles remain in the visualization plane long enought for their paths to be followed.

Figure 19 shows good agreement between the computed streamlines (figure 19*a*) and the experimental flow visualization (figure 19*b*) in the meridional plane. The visualization shows an example of particle paths obtained for $Re = 26$, $z \approx 0.5$. The higher and lower parts of the visualization correspond to the two rotating disks. The fixed sidewall is on the right-hand side, but the centre of the cell is not included in the picture, thus only a part of its radial extent is represented. The trace of an unsteady structure can be observed in the centre of the picture and its wavelength can be evaluated to approximately $\lambda = 2.3$, which is very close to the value $\lambda = 2.5$ predicted by calculations. The right-hand side of the figure, close to the fixed sidewall, shows more complex disturbances; their patterns vary as a function of time. The figure shows good agreement between calculations (figure 19*a*) and visualizations (figure 19*b*).
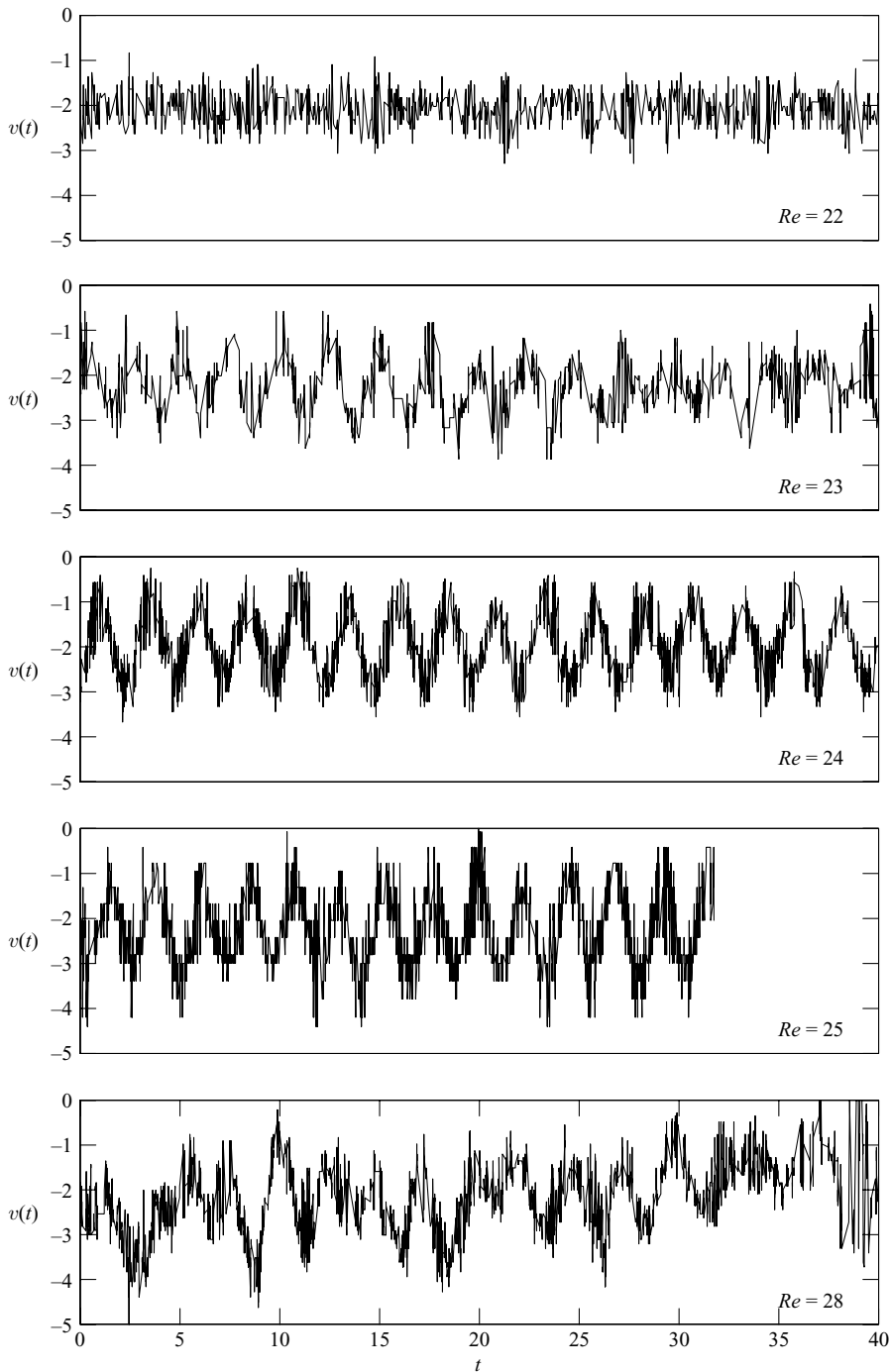
FIGURE 18. Tangential velocity $v(t)$ measurements as a function of the dimensionless time $t = \omega^* t^*$ for different Re with $r = 12; z = 0.42; s = -1; R = 15$.

As previously stated, visualizations in a midplane parallel to the disks are easier to obtain. For $s = -1$, the particles at $z = 0.5$ remain in the light sheet long enough for their trajectories to be observed without too much difficulty. Observation shows
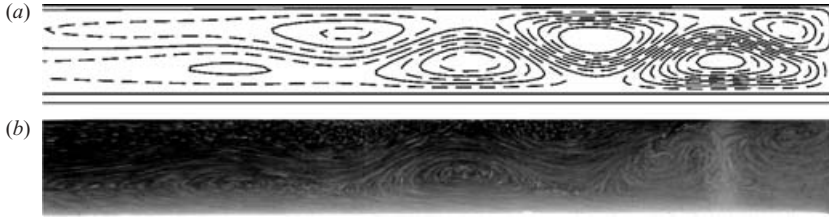
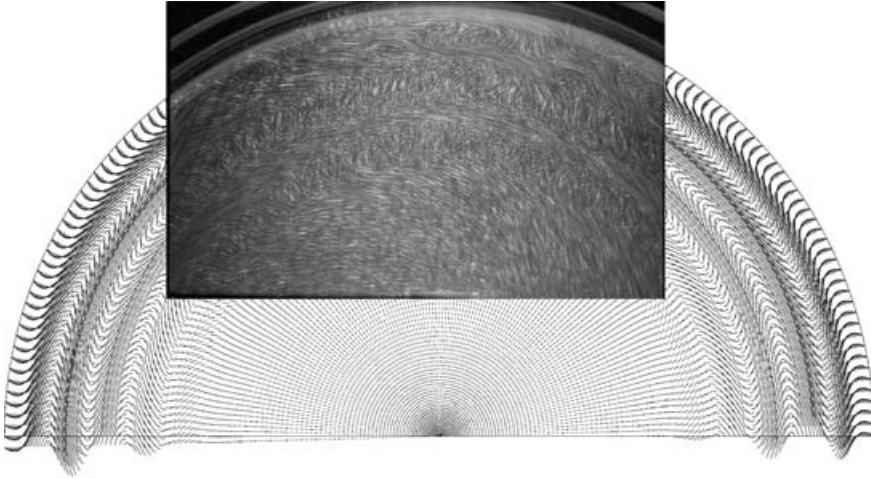FIGURE 19. (*a*) Meridional flow streamlines and (*b*) visualization. $Re = 26$; $s = -1$; $R = 15$.

FIGURE 20. Visualization and corresponding trajectory field computed in the midplane between disks at $z = 0.5$. $Re = 26$, $s = -1$, $R = 15$, exposure time $t^* \approx 1$ s.

the appearance of an instability for $Re = 24$. This formation of a train of centrifugal axisymmetric waves can be seen. However, the limitations imposed by the experimental device prevent the exploration of a wide range of Reynolds numbers. Unsteady three-dimensional disturbances, already noted in meridional views, disturb the axisymmetry of the wave train near the fixed sidewall and this increases significantly with Reynolds number. This loss of axisymmetry near the fixed sidewall can be attributed either to experimental device imperfections or to the appearance of three-dimensional unsteady disturbances beyond a critical radius. It is not possible to settle this question with the tools used here. The best solution would be to use an unsteady three-dimensional Navier–Stokes code to determine whether non-axisymmetric instabilities appear for these parameter values. Axisymmetric instabilities appear in the vicinity of $r/R \cong 0.5$ and displace towards the periphery while being increasingly disturbed by three-dimensional modes. It is for $Re \in [25, 26]$ that waves are easiest to observe, as they preserve their axisymmetry in most of the area. Three-dimensional disturbances are then very weak and not yet clearly visible; they appear randomly, close to the sidewall.

Figure 20 shows the superposition of a photograph (aperture 5.6, shutter 1s) taken in the midplane ($z = 0.5$) for $Re = 26$, and of the layout of portions of trajectories calculated in the same plane, throughout the opening time of the camera. The two pictures show good agreement between calculations and visualizations, even though the experimental apparatus prevents the observation of the whole light sheet. The photographs show the trace of the axisymmetric wavetrain in most of the field, but

also more complex structures close to the sidewall, demonstrating the existence of the three-dimensional effects already mentioned.

As shown in §3.2.2, axisymmetric disturbances invade the whole of the cavity (cf. 11*b*). Visualizations show axisymmetric instabilities only beyond $r/R \cong 0.5$ because of the necessarily limited sensitivity of the experimental technique, which does not mean that the instabilities are not present in the whole of the cavity.

Using visualizations and velocity measurements, it is possible to calculate the wavelength and the period of the disturbance. For $Re = 26$, we can estimate the wavelength at $\lambda = 2.3 \pm 0.2$ and the period to be $T = 2.5 \pm 0.1$. These values are in agreement with the computations ($\lambda = 2.5$ and $T = 2.63$) and thus confirm the existence of axisymmetric instabilities for very low values of Re.

4. Conclusion

We have studied the onset of the first axisymmetric instabilities between two coaxial disks enclosed in a stationary sidewall. If the cavity thus formed is of large aspect ratio $R = R^*/e^*$, the flow can be described by the self-similar von Kármán solutions in most of the field.

These self-similar solutions are found to be unstable with respect to infinitesimal unsteady disturbances. For moderate Reynolds number values ($Re \leqslant 50$) and for all rotation ratios $s \in [-1, 1[$, there is a critical local radius r_{pc} beyond which centrifugal axisymmetric waves invade the entire space between the disks. In the case of slightly counter-rotating disks ($s \in [-0.56, 0[$), two different travelling waves (i.e. defined by two different wavenumbers and two different frequencies: types I and II) appear for the same critical value of the local radius r_{pc}.

A spatio-temporal stability analysis shows that for the few cases treated here, the disturbances become absolutely unstable (AI) for values very close to the critical radius found by temporal analysis. Although this is not a systematic study, it would seem to indicate that this result can be generalized within the range of the examined parameters $Re \leqslant 50$ and $s \in [-1, 1[$. It is known that the onset of a locally absolutely unstable mode can indicate the existence of global instability. In the case of slightly counter-rotating disks ($s \in [-0.56, 0[$), of the two modes found to be unstable, type I becomes absolutely unstable (AI) (for a value very close to the critical radius $r_{pc}^{\bullet}$), whereas type II remains convectively unstable (CI).

A general study would be required to analyse this behaviour for a larger range of parameters and to try to establish a connection between the observations described here and the destabilization of this type of flow in the boundary-layer regime.

Subsequently, direct axisymmetric computations showed that unsteady solutions, found here in the case of infinite disks, can appear inside a cavity, that is to say between two disks enclosed within a fixed sidewall. In order for this to be the case, the critical radius r_{pc} must be included in the zone where the flow can be described by the self-similar solutions. Computations confirm the destabilization of the basic flow by a centrifugal global mode which affects the whole cavity. This unstable global mode has the characteristics (wavelength, period and phase velocity) of the mode found to be unstable for the same parameter values in the case of infinite disks.

In a cavity, these instabilities are particularly difficult to calculate because of the high value of the critical radius r_{pc} beyond which the self-similar solutions become unstable, and which must necessarily be included in the investigated field. It is clear that the smaller the aspect ratio of the cavity, the higher the critical Reynolds number must be, a behaviour which is not compatible with the maintenance in the cavity of

a zone where the flow is well represented by self-similar solutions. Some calculations showed that the limit at which this type of instability no longer appears on this side may be estimated at $R \approx 10.3$. This implies that such an instability can be observed only in cavities of large aspect ratio R.

This work constitutes a first step which should be continued by a three-dimensional study in order to determine if axisymmetric instabilities calculated here are actually those which destabilize the flow or if, for at least part of the explored parameters, three-dimensional structures coexist, or even take precedence. It is undoubtedly the nature, AI or CI, of potential three-dimensional instabilities which would make it possible to determine this. It could also be interesting to specify the evolution of these instabilities as the Reynolds number increases even more. In particular, the passage from centrifugal axisymmetric instabilities described here to axisymmetric and three-dimensional instabilities in the boundary layers described in the literature for higher values of the Reynolds number remains to be detailed.

Finally, an experimental study performed in a cavity of aspect ratio $R = 15$ confirms the existence of an axisymmetric centrifugal disturbance for values very close to the predictions. This experimental work should be supplemented by continuing the exploration of the parameter ranges (i.e. Re and s) to reach notably higher Re values, largely explored in the literature. Again, it is the connection between instabilities presented here and the already well-known boundary-layer instabilities which remains to be established. In addition, experimental study has highlighted the existence of three-dimensional unsteady structures at the periphery of the disks. It would be interesting to know, for example, following the work of Nore *et al.* (2006) using non-axisymmetric computations, how the competition between all of these unstable modes takes place and if there is a critical radius for the onset of these three-dimensional instabilities or if, as for axisymmetric instabilities described here, their absolutely unstable nature leads them to invade the entire cavity.

REFERENCES

BATCHELOR, K. 1951 Note on a class of solutions of the Navier–Stokes equations representing steady rotationally-symmetric flow. *Q. J. Mech. Appl. Maths* **4**, 29–41.

BERS, A. 1975 Linear waves and instabilities. In *Physique des Plasmas* (ed. C. DeWitt & J. Peyraud), pp. 117–215. Gordon & Breach.

BÖDEWADT, U. 1940 Die drehströmung über festem grunde. *Z. Angew. Math. Mech.* **20**, 241.

BRIGGS, R. 1964 *Electron-Stream Interaction with Plasma*. MIT Press.

COUSIN-RITTEMARD, N., DAUBE, O. & LE QUÉRÉ, P. 1998 Sur la nature de la première bifurcation des écoulements interdisques. *C. R. Acad. Sci. Paris* **IIb** (326), 359.

COUSIN-RITTEMARD, N., DAUBE, O. & LE QUÉRÉ, P. 1999 Structuration de la solution stationnaire des écoulements interdisques en configuration rotor–stator. *C. R. Acad. Sci. Paris* **IIb** (327), 221.

DELBENDE, I., CHOMAZ, J.-M. & HUERRE, P. 1998 Absolute/convective instabilities in the Batchelor vortex: a numerical study of the linear impulse response. *J. Fluid Mech.* **355**, 229–254.

FALLER, A. J. & KAYLOR, R. E. 1966 A numerical study of the instability of the laminar Ekman boundary layer. *J. Atmos. Sci.* **23**, 466.

GAUTHIER, G., GONDRET, P. & RABAUD, M. 1999 Axisymmetric propagating vortices in the flow between a stationary and a rotating disk enclosed by a cylinder. *J. Fluid Mech.* **386**, 105–126.

GAUTHIER, G., GONDRET, P., MOISY, F. & RABAUD, M. 2002 Instabilities in the flow between co- and counter-rotating disks. *J. Fluid Mech.* **473**, 1–21.

GREGORY, N., STUART, J. & WALKER, W. 1955 On the stability of three-dimensional boundary layers with application to the flow due to a rotating disk. *Phil. Trans. R. Soc. Lond* **248**, 155–199.

HEALEY, J. 2004 On the relation between the viscous and inviscid absolute instabilities of the rotating-disk boundary layer. *J. Fluid Mech.* **511**, 179–199.

HILL, R. & BALL, K. 1997 Chebyshev collocation analysis of axisymmetric flow and heat transfer between counter-rotating disks. *Trans. ASME* I: *J. Fluids Engng* **119**, 940–947.

HOLODNIOK, M., KUBICEK, M. & HLAVACEK, V. 1977 Computation of the flow between two rotating coaxial disks. *J. Fluid Mech.* **84**, 689.

HOLODNIOK, M., KUBICEK, M. & HLAVACEK, V. 1981 Computation of the flow between two rotating coaxial disks: multiplicity of steady-state solutions. *J. Fluid Mech.* **108**, 227.

HUERRE, P. 2000 Open shear flow instabilities. In *Perspectives in Fluid Dynamics–A Collective Introduction to Current Research* (ed. G. K. Batchelor, H. K. Moffat & M. G. Worster), chap. 4. Cambridge University Press.

HUERRE, P. & MONKEWITZ, P. A. 1990 Local and global instabilities in spatially developing flows. *Annu. Rev. Fluid Mech.* **22**, 473–537.

IGLESIAS, I. & HUMPHREY, J. 1998 Two- and three-dimensional laminar flows between disks co-rotating in a fixed cylindrical enclosure. *Intl J. Numer. Meth. Fluids* **26**, 581.

JARRE, S., LE GAL, P. & CHAUVE, M.-P. 1991 Experimental analysis of the instability of the boundary layer over a rotating disk. *Europhys. Lett.* **14**, 649–654.

JARRE, S., LE GAL, P. & CHAUVE, M.-P. 1996 Experimental study of a rotating disk instability. I. Natural flow. *Phys. Fluids* **8**, 496–508.

VON KÁRMÁN, T. 1921 Über laminare und turbulente reibung. *Z. Angew. Math. Mech.* **1**, 233–251.

LINGWOOD, R. 1995 Absolute instability of the boundary layer on a rotating disk. *J. Fluid Mech.* **299**, 17–33.

LINGWOOD, R. 1996 An experimental study of absolute instability of the rotating-disk boundary-layer flow. *J. Fluid Mech.* **314**, 373–405.

LOPEZ, J. M., HART, J., MARQUES, F., KITTELMAN, S. & SHEN, J. 2002 Instability and mode interactions in a differentially-driven rotating cylinder. *J. Fluid Mech.* **462**, 383–409.

MELLOR, G., CHAPPLE, P. & STOKES, V. 1968 On the flow between a rotating and a stationary disk. *J. Fluid Mech.* **31**, 95–112.

MOISY, F., DOARÉ, O., PASUTTO, T., DAUBE, O. & RABAUD, M. 2004 Experimental and numerical study of the shear layer instability between two counter-rotating disks. *J. Fluid Mech.* **207**, 175–202.

NGUYEN, N., RIBAULT, J. & FLORENT, P. 1975 Multiple solutions for flow between coaxial disks. *J. Fluid Mech.* **68**, 369.

NORE, C., TUCKERMAN, L. S., DAUBE, O. & XIN, S. 2003 The 1:2 mode interaction in exactly counter-rotating von Kármán swirling flow. *J. Fluid Mech.* **477**, 51–88.

NORE, C., TARTAR, M., DAUBE, O. & TUCKERMAN, L. S. 2004 Survey of instability thresholds of flow between exactly counter-rotating disks. *J. Fluid Mech.* **511**, 45–65.

NORE, C., MARTIN-WITKOWSKI, L., FOUCAULT, E., PÉCHEUX, J., DAUBE, O. & LE QUÉRÉ, P. 2006 Competition between axisymmetric and three-dimensional patterns between exactly counter-rotating disks. *Phys. Fluids* **18**, 054102.

OWEN, J. & ROGERS, R. 1989 *Flow and Heat Transfer in Rotating Disc Systems, vol. 1 : Rotor–Stator Systems*. Morris WD, Somerset, England: Research Studies.

REED, H. & SARIC, R. 1989 Stability of three-dimensional boundary layers. *Annu. Rev. Fluid Mech.* **21**, 235–284.

SAN'KOV, P. & SMIRNOV, E. 1992 Stability of viscous flow between rotating and stationary disks. *Fluid Dyn.* **26**, 857–864.

SARIC, R., REED, H. & WHITE, E. 2003 Stability and transition of three-dimensional boundary layers. *Annu. Rev. Fluid Mech.* **35**, 413–440.

SCHOUVEILER, L., LE GAL, P. & CHAUVE, M. 1998 Stability of a traveling roll system in a rotating disk flow. *Phys. Fluids* **10**, 2695–2697.

SCHOUVEILER, L., LE GAL, P., CHAUVE, M. & TAKEDA, Y. 1999 Spiral and circular waves in the flow between a rotating and a stationary disk. *Exps. Fluids* **26**, 179–187.

SCHOUVEILER, L., LE GAL, P. & CHAUVE, M. 2001 Instabilities of the flow between a rotating and a stationary disk. *J. Fluid Mech.* **443**, 329–350.

SERRE, E., CRESPO DEL ARCO, E. & BONTOUX, P. 2001 Annular and spiral patterns in flows between rotating and stationary discs. *J. Fluid Mech.* **434**, 65–100.

STEWARTSON, K. 1953 On the flow between two rotating coaxial disks. *Proc. Camb. Phil. Soc.* **49**, 333–341.

SZERI, A., SCHNEIDER, S., LABBE, F. & KAUFMAN, H. 1983a Flow between rotating disks. Part 1. Basic flow. *J. Fluid Mech.* **134**, 103–131.

SZERI, A. Z., GIRON, A., SCHNEIDER, S. J. & KAUFMAN, H. N. 1983b Flow between rotating disks. Part 2. Stability. *J. Fluid Mech.* **134**, 133–154.

SZETO, R. K.-H. 1978 The flow between rotating coaxial disks. PhD thesis, California Institute of Technology.